Optically induced dynamics in nematic liquid crystals: The role of finite beam size

E. Brasselet*
Laboratoire de Photonique Quantique et Moléculaire, Ecole Normale Supérieure de Cachan, 94235 Cachan Cedex, France

B. Doyon and T. V. Galstian†
Département de Physique, de Génie Physique, et d'Optique, Université Laval, Cité Universitaire, Québec, Canada G1K 7P4

L. J. Dubé‡
Laboratoire de Dynamique des Ions, des Atomes, et des Molécules, Université Pierre et Marie Curie, 4 Place Jussieu, 75252 Paris Cedex 05, France

(Received 22 February 2003; revised manuscript received 9 July 2003; published 10 February 2004)

We report on the influence of a finite beam size on the molecular reorientation dynamics when a nematic liquid crystal film is excited by a laser beam. We present experimental evidence of a new class of nonlinear dynamics when the excitation is a Gaussian shaped, circularly polarized laser beam at normal incidence. Various nonlinear regimes, periodic, quasiperiodic, intermittent, and possibly chaotic, are observed. A physical interpretation based on walk-off effects is proposed and its implications on current research in the field are discussed.

DOI: 10.1103/PhysRevE.69.021701 PACS number(s): 42.70.Df, 42.65.−k, 61.30.Gd

I. INTRODUCTION

Liquid crystals offer a versatile system for the experimental and theoretical study of a variety of nonlinear phenomena. In particular, the nonlinear optics of liquid crystals has become a well-established research field [1–4] including light-induced phase transitions [1,5,6] and stimulated light scattering [7]. In the past decade, considerable efforts have been made to achieve a better understanding of nonlinear mechanisms of the light–liquid crystal interaction. The case of a homeotropic cell of nematic liquid crystal (NLC) under a light field excitation has received special attention and the ensuing studies have led to quantitative theoretical descriptions capable of retrieving the main features of the various dynamical regimes studied until then. For instance, we can mention the case of the normally incident elliptically polarized light leading to a rich variety of molecular dynamics [8,9] together with the particular case of circularly polarized excitation which exhibits a nontrivial sequence of successive bifurcations [10,11]. The transition to chaos via a cascade of gluing bifurcations by an ordinary wave at oblique incidence [12–17] is yet another example. More recently, it was shown that a strongly astigmatic laser beam can induce nonlinear oscillations when spin and orbital angular momentum of light are in competition [18]. In particular, chaotic rotation associated with intermittency was identified in that case [19]. However, due to the complexity of the problem, most of the corresponding theoretical models have assumed an infinite plane wave (IPW) excitation, an assumption not justified in many experiments where the beam size is comparable to or less than the NLC film thickness. Despite several attempts to describe the finite beam size effects, only the linearly polarized excitation, where the long-term behavior is time independent, has been studied in some detail [5,20–24] and it is fair to say that a complete dynamical model is still lacking.

In a recent study [11], we have pointed out the role of longitudinal asymmetry (along the propagation direction) and twisted deformations (three dimensional) in the case of circularly polarized excitation at normal incidence. This has brought us to the following suggestion. In spatially confined beams, transverse effects should compete with the longitudinal ones when the beam size is small enough and should eventually generate novel dynamics. The present contribution is devoted to following questions. When are finite beam size effects significant? Does the dynamics qualitatively change when the beam size is reduced and, if yes, what is the nature of the dynamics produced? To be specific, we have chosen to limit our demonstration to the case of a Gaussian shaped laser beam with circular polarization incident at normal incidence.

The paper is organized as follows. Section II presents the experimental setup used to probe finite beam size effects on the light-induced reorientation dynamics. It is shown that the aspect ratio between the beam size and the cell thickness provides a bifurcation parameter for a new class of optically induced nonlinear dynamics. Section III explores in detail the dynamical scenario for strongly confined beams when the excitation intensity is taken as the bifurcation parameter. For instance, a transition from a quasiperiodic to a possibly chaotic regime is identified. In Sec. IV, prospective comments on the crucial role of finite beam size effects in other interaction geometry and experimental and theoretical consequences are reviewed. Finally, our conclusions are summarized in Sec. V.

*Corresponding author. Email address: ebrassel@lpqm.ens-cachan.fr

†TVG is a member of the Center d'Optique, Photonique, et Laser, Université Laval, Québec, Canada and also with Photintech Inc., 1245 Chemin Ste-Foy, Québec, Canada.

‡Also at Département de Physique, de Génie Physique, et d'Optique, Université Laval, Cité Universitaire, Québec, Canada G1K 7P4.

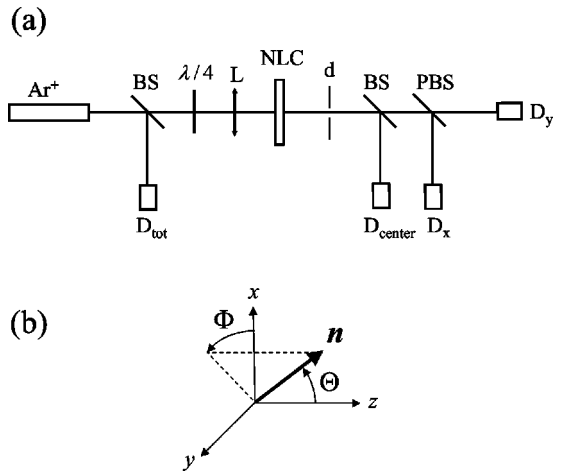

FIG. 1. (a) Experimental setup. Ar^+, argon ion laser operating at 514 nm; BS, beam splitter; λ/4, quarter wave plate; L, lens; NLC, nematic liquid crystal film; d, diaphragm; PBS: polarizing beam splitter; D_i, photodetectors. (b) Definition of the director $\boldsymbol{n}$. The director's orientation is given by the spherical angles (Θ,Φ) defined as $\Theta=\angle(\boldsymbol{e}_z,\boldsymbol{n})$ and $\Phi=\angle(\boldsymbol{e}_x,\boldsymbol{n}-\boldsymbol{n}_z)$ where $(\boldsymbol{e}_x,\boldsymbol{e}_y,\boldsymbol{e}_z)$ is the Cartesian coordinate system.

We will refer to the molecular dynamics by means of the vector field that represents the average local orientation of the molecules defined by the unit vector $\boldsymbol{n}(x,y,z,t)$, called the director. Its orientation is given by the two usual spherical angles Θ and Φ, namely, $\boldsymbol{n}=(\sin\Theta\cos\Phi,\sin\Theta\sin\Phi,\cos\Theta)$ [see Fig. 1(b)].

II. REORIENTATION DYNAMICS CONTROLLED BY FINITE BEAM SIZE

A. Experiment

The sample is a film of nematic liquid crystal E7 enclosed between two glass substrates located at $z=0$ and $z=L$ ($=50$ or 100 μm). The substrates are coated with CTAB surfactant for strong homeotropic alignment, i.e., an alignment perpendicular to the surfaces of the plates. The pumping laser beam is obtained from an Ar^+ laser (operating at 514 nm in the TEM_{00} mode) and is focused at normal incidence on the sample by the lens L [see Fig. 1(a)]. At the sample location the intensity profile has a Gaussian shape $G_{w_0}(x,y)\propto\exp[-2(x^2+y^2)/w_0^2]$ and we define $d=2w_0$ as the beam diameter where the central intensity has dropped by a factor e^{-2}. Our experiments have been performed with different focal lengths from $f=10$ up to 25 cm corresponding to beam diameters from $d=24$ to 67 μm. The polarization state of the excitation light is made circular using a quarter wave plate (λ/4) placed before the lens L [see Fig. 1(a)]. The director dynamics is retrieved by the analysis of the central part of the emerging excitation beam after the diaphragm d. Photodiodes D_{center}, D_x, and D_y collect, respectively, the total intensity of the central part of the beam emerging from the sample, I_{center}, and the corresponding vertical and horizontal components of the electric field, I_x and I_y ($I_{\text{center}}=I_x+I_y$). The excitation intensity I_{tot} is monitored with the photodiode D_{tot}. Data acquisition frequency is 5 Hz in all experiments and the increment of normalized excitation intensity is $\delta\tilde{I}=0.05$, where $\tilde{I}=I_{\text{tot}}/I_F$, and I_F denotes the Fréedericksz transition threshold.

The time series $I_{\text{center}}(t)$ contains explicit information on Θ only. This can be seen from the two connected facts that the amplitude of self-focusing arising from finite beam size is governed by the amount of reorientation (Θ) and that only part of the total output intensity is collected by D_{center}. On the other hand, the time series $I_x(t)$ and $I_y(t)$ contain explicit information on both Θ and Φ since the intensities of the x and y electric field components depend on both the shape (Θ) and the position (Φ) of the output polarization ellipse and on I_{center}. The normalized intensities with respect to I_{center}, $i_x(t)\equiv I_x/I_{\text{center}}$ and $i_y(t)\equiv I_y/I_{\text{center}}$, contain for their part only explicit information on the polarization ellipse. Since $i_x(t)=1-i_y(t)$, these time series possess the same dynamical information, we shall refer to any of these quantities as $i(t)$.

Figure 2 shows the phase space reconstructed from the observed time series, namely, $i(t+\tau)$ versus $i(t)$ where τ is a time delay, as function of $\tilde{I}$, and the ratio $\delta\equiv d/L=2w_0/L$. The time delay is chosen conventionally as the first zero of the autocorrelation function

$$C(\tau)=T^{-1}\int_0^T f(t)f(t+\tau)dt,$$

where $f(t)$ is the time series and T its duration. The shapes observed in Fig. 2 are easily interpreted. A fine closed loop in phase space is the sign of a uniform precession regime without nutation, i.e., the polarization ellipse is continuously rotating while keeping its shape constant. A *time dependent* shape of the polarization ellipse is signaled on the other hand by a thickening of the closedloop. For example, in the second line of Fig. 2, the nutation amplitude is almost negligible until $\tilde{I}=1.25$ is reached where significant nutation abruptly appears. This corresponds to the *secondary instability* observed in Ref. [10] whose bifurcation point was labeled $\tilde{I}=\tilde{I}_B$. The important feature in this set of graphs is that the geometrical aspect ratio δ may be considered as a bifurcation parameter since a transition from a low to a large nutation regime is clearly visible as δ is decreased ($\tilde{I}=$ const).

It therefore appears that the roles of $\tilde{I}$ and δ are similar since by keeping $\tilde{I}$ fixed and decreasing δ, one reveals a sequence of dynamical regimes in many points identical to that obtained by using $\tilde{I}$ as the bifurcation parameter. This can be seen by comparing the ith line with the ith column of Fig. 2. This does *not* imply, as we will shortly see, that the *same* final dynamical state is reached through the *same* series of instability mechanisms as one travels horizontally or vertically in parameter space $(\tilde{I},\delta)$.

B. Discussion

A number of physical quantities vary as the value of δ is changed keeping $\tilde{I}$ fixed. The most prominent of these are (i) the amount of longitudinal nonuniformity, (ii) the local angle of incidence, and also (iii) the total intensity. These quanti-

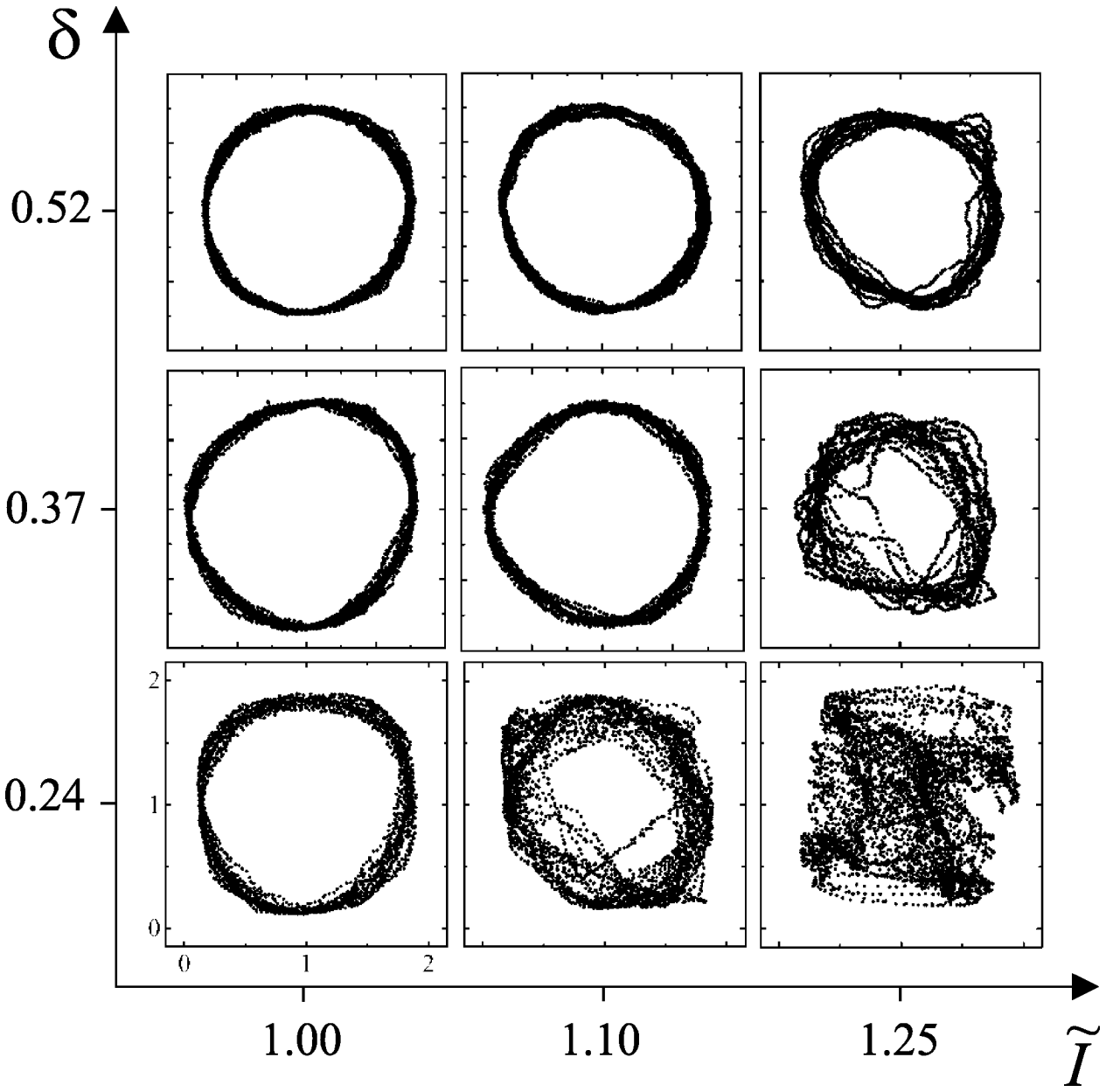

FIG. 2. Curves in each square represent the experimental reconstructed phase space $i(t+\tau)$ vs $i(t)$ for various values of the normalized intensity $\tilde{I}$ and the geometrical ratio $\delta=2w_0/L$ for a cell thickness $L=100\ \mu$m. The time delay τ is 8, 10, and 11 s for $\delta=0.24$, 0.37, and 0.52, respectively.

ties are already known to generate complex dynamics as recently documented in a circularly polarized excitation experiment [points (i) and (iii)] in Ref. [11] and in the transition to chaos under ordinary light field at oblique incidence [points (ii) and (iii)] [15–17,25–27]. It is now left to quantify the relative importance of the variations induced on these quantities by changes in δ.

(i) Due to the Gaussian nature of the beam, the light intensity is nonuniform along the direction of propagation. We define in Fig. 3 $w(z)$ as the beam cross section radius at e^{-2} of the central intensity and we denote its relative variation by $\delta w(z)/w_0 \equiv [w(z)-w_0]/w_0$. One can verify that the beam cross section is well approximated by a cylinder of radius w_0 since $\delta w(z)/w_0 \ll 1$ within the sample for all cases studied.

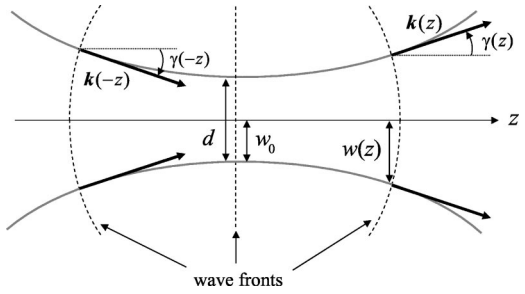

FIG. 3. Gaussian beam structure near the beam waist. Dotted lines are wave fronts and solid lines refer to the beam radius $w(z)$. The wave vector $\boldsymbol{k}$ and its angle γ with the propagation axis z are represented at $-z$ and z, respectively.

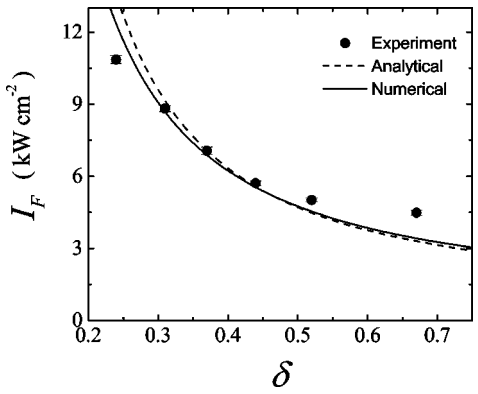

FIG. 4. Experimental Fréedericksz transition threshold (dots) vs δ for a cell thickness $L=100$ μm. The dashed line corresponds to the analytical solution of Ref. [6] and the full line is obtained from the numerical solution presented in the Appendix. The only adjustable parameter is the value I_F^{∞} at $\delta\rightarrow\infty$; it agrees in both cases to within a few percent.

Therefore, it is safe to conclude that the nonuniformity in intensity along the *z* axis will have little effect on the dynamics and cannot explain the results of Fig. 2 .

(ii) Also in Fig. 3, we see that the wave vector $\boldsymbol{k}$ makes an angle γ with the propagation axis *z* which depends on both *z* and the distance *r* from the *z* axis. Under our operating conditions, the maximum *local* angle of incidence $\gamma(z)$ calculated at $r=w(z)$ is smaller than 10^{-2} deg within the sample. In contrast, complex dynamical behavior arising from an oblique incident excitation occurs for angles of the order of few degrees [15–17,25–27]. Here again, the deviation from normal incidence due to the Gaussian structure of the excitation beam cannot explain our observations.

(iii) It is well known that the Fréedericksz threshold intensity I_F depends on δ. Figure 4 shows I_F as function of δ for $L=100$ μm (circles). The dashed and full lines correspond to theoretical estimates detailed in the Appendix. The variation of I_F is quite sizable over the range of δ displayed and therefore to keep $\tilde{I}$ fixed when δ is decreased, the total intensity I_{tot} must increase proportionally. To examine the dynamical changes induced by the increase in total energy, we have produced experimentally two time series taken at constant $\tilde{I}=1.15$ with fixed $2w_0=24$ μm and different *L* (50 μm and 100 μm). These conditions imply $\delta=0.48$ and 0.24, respectively. Figure 5 displays the reconstructed phase space obtained from the experimental $i(t)$. Although the total intensity for the $L=50$ μm cell is more than twice that for the 100 μm one (recall that $I_F\propto 1/L^2$), the dynamics is still that of a low nutation regime for the first cell [$\delta=0.48$, Fig. 5(a)] in stark distinction to the second one [$\delta=0.24$, Fig. 5(b)]. Thus it appears that it is the value of δ rather than I_{tot} that governs the transition from low to large nutation regime at fixed $\tilde{I}$.

In summary, when the excitation beam diameter is smaller than the cell thickness, we have identified δ as the bifurcation parameter for a new class of optically induced dynamics in NLC.

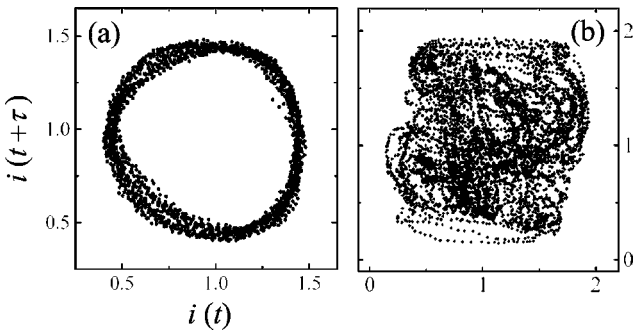

FIG. 5. Experimental reconstructed phase space $i(t+\tau)$ vs $i(t)$ at $\tilde{I}=1.15$. (a) $\delta=0.48$, $L=50$ μm with $\tau=2.5$ s; (b) $\delta=0.24$, $L=100$ μm with $\tau=8$ s.

C. Drift of the secondary instability

We see from Fig. 2 that when δ is decreased, the transition from a low to a large nutation regime appears correspondingly at lower intensities. We have extended our measurements to more values of δ and Fig. 6 presents the bifurcation line associated with the transition from uniform precession to nonuniform precesison nutation regime in the plane $(\delta,\tilde{I})$ for $\delta<0.7$. We see that large variation appears typically in the range $0.3<\delta<0.5$. The saturation effect observed for the smallest δ is interpreted by the fact that the transverse reorientation profile fails to follow the decrease of the beam size due to elasticity (transverse nonlocality). Physically, this can be understood by recalling that in the limit of small δ, $I_{\mathrm{tot}}\propto 1/w_0^2$ (see the Appendix) while the power injected in the system, $P=\pi w_0^2 I_{\mathrm{tot}}$, becomes independent of the beam size. On the other hand, the saturation observed for the largest δ agrees with the theoretical IPW limit $\tilde{I}_B(\delta\rightarrow\infty)\simeq 1.44$ calculated in Ref. [11]. However, for higher values of δ, the system is found rather unstable in the sense that large orientational fluctuations are eventually observed (as reported in Ref. [28]) and significant nutation appears correspondingly at lower intensities in agreement with the reported experimental value of $\tilde{I}_B=1.25\pm0.05$ observed at $\delta\simeq 0.75$ [10,35].

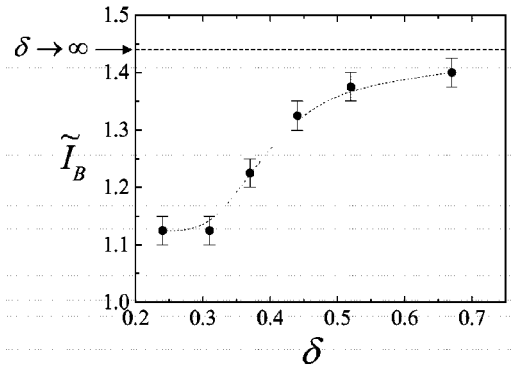

FIG. 6. Experimental secondary instability threshold (dots) vs δ for a cell thickness $L=100$ μm. The dotted line is meant to guide the eye. The dashed line represents the infinite plane wave limit, $\tilde{I}_B^{\infty}$.

We conclude from this study that important dynamical effects due to finite beam size occur for small δ while the dynamical behavior of the system is qualitatively the same just above the primary instability (Fréedericksz transition).

III. NONLINEAR DYNAMICS SCENARIO

It is now instructive to follow the evolution of the dynamics as the normalized intensity $\tilde{I}$ is varied for a given δ.

A. Scenario for $\delta \to \infty$: Infinite plane wave model

In two recent contributions [10,11], we have developed an IPW theoretical model that describes quantitatively the dynamical scenario of a nematic liquid crystal cell with strong homeotropic alignment under a circularly polarized light excitation at normal incidence. As $\tilde{I}$ is increased, it has been shown that the system undergoes a subcritical Hopf bifurcation at $\tilde{I}=1$. In the range $1<\tilde{I}<\tilde{I}_B$ the director dynamics exhibits a limit cycle behavior that corresponds to quasiuniform precession ($\partial_t \Phi \approx \Omega$ where Ω is the precession angular velocity) with small nutation ($\delta\Theta/\Theta \ll 1$) around the propagation direction. As $\tilde{I}$ is further increased in the range $\tilde{I}_B<\tilde{I}<\tilde{I}^*$, the dynamics corresponds to a nonuniform precession [$\delta(\partial_t\Phi)/\partial_t\Phi \sim 1$] coupled to a large nutation ($\delta\Theta/\Theta \sim 1$). Finally, when $\tilde{I}>\tilde{I}^*$ the system is strongly reoriented ($\Theta^2 \sim 1$) in contrast to the previous regimes where the amplitude of reorientation is small ($\Theta^2 \ll 1$).

For the present study, we have made a series of calculations based on Ref. [11] that cover the intensity range $1<\tilde{I}<\tilde{I}^*$. Apart from being of interest in their own right, these calculations provide us with a reference (at $\delta \to \infty$) against which we intend to measure the effects of a finite beam size on the dynamics. The theoretical results obtained by retaining four modes of reorientation are summarized in Fig. 7. The reconstructed phase space $I_{x,y}(t+\tau)$ versus $I_{x,y}(t)$ are presented on the left. On the right part of this figure, the Fourier power spectra of the total phase shift $\Delta(t) = k_0 \int_0^L [n_e(z,t) - n_o] dz$ between *o* and *e* waves at the output of the cell, where n_o and n_e are the *o* and *e* refractive index, respectively, and of $I_{x,y}(t) = |E_{x,y}(L,t)|^2$ are displayed. The frequency labeling reflects the dependence of these observables on the independent variables of the theory, namely, Θ and Φ.

For $\tilde{I}<1$, we have no reorientation, as expected. At $\tilde{I}=1$, the system experiences a subcritical Hopf bifurcation that corresponds to the Fréedericksz transition and, after a transient, the director settles to a stationary uniform precession regime with frequency f_0. In that case, the phase space is a perfect circle [Fig. 7(a)] and the Fourier spectra $I_{x,y}(\omega)$ exhibit a single frequency $2f_0$ since the polarization ellipse is invariant by a rotation of π around the *z* axis. This uniform precession regime is observed for $1<\tilde{I}<1.44$ and, at higher intensities, the system explores a progressively larger volume of phase space [Figs. 7(b) and 7(c)], which indicates the presence of nutation. A look at the reconstructed phase space for $\tilde{I}=1.45$ indicates that a dynamical transition has just taken place (we have reported this transition at $\tilde{I}=\tilde{I}_B \simeq 1.44$ in Ref. [11]). A new frequency labeled f_1 suddenly appears in the system through this transition, which has the character of a supercritical Hopf bifurcation. This frequency is clearly identified from the Fourier spectra [Fig. 7(c)] just above the corresponding threshold. The NLC molecules are now rotating around the *z* axis with frequency f_0 with a large periodic nutation with frequency f_1, which is a precession-nutation regime. This continuous transition from a periodic regime towards quasiperiodicity emphasizes the second-order nature of the transition. On the other hand, the occurrence of the harmonics $f_1 \pm 2f_0$ in the spectra $I_{x,y}(\omega)$ is a direct manifestation of the nonlinear coupling between the two degrees of freedom Θ and Φ. A further increase of $\tilde{I}$ strengthens the nonlinear coupling between Θ and Φ as demonstrated by Fig. 7(d) where the harmonics $f_1 \pm 2f_0$ now make an important contribution to the spectra $I_{x,y}(\omega)$. In addition, the nonlinear character of the nutation dynamics is observed in the spectrum $\Delta(\omega)$ through the appearance of the second harmonic $2f_1$. This allows the identification of two additional frequencies in the spectrum $I_{x,y}(\omega)$, namely, the harmonics $2f_1 \pm 2f_0$. Higher harmonics nf_1 and $nf_1 \pm 2f_0$, n integer [Figs. 7(c)–7(e)], become more and more visible as the intensity is further increased until, at $\tilde{I}=\tilde{I}^*=1.75$, a first-order transition to a large reoriented state associated with a giant hysteretic behavior occurs [11].

B. Scenario for finite δ: Experiment

Before confronting experiment and theory, a careful choice of the corresponding dynamical quantities is required. Following our previous discussion, the experimental time series $I_{\text{center}}(t)$ may be related to $\Delta(t)$ while the experimental $i(t)$ corresponds to the theoretical $I_{x,y}(t)$. Indeed, both $I_{\text{center}}(t)$ and $\Delta(t)$ possess explicit information on Θ only, while $i(t)$ and the theoretical $I_{x,y}(t)$ are free from self-focusing effects.

1. Periodic, quasiperiodic, and irregular regimes

Figure 8 summarizes the experimental dynamics when $\delta=0.24$ for $\tilde{I} \leqslant 1.25$. The reconstructed phase space $i(t+\tau)$ versus $i(t)$ is presented on the left. On the right part of this figure, the Fourier power spectra $I_{\text{center}}(\omega)$ and $i(\omega)$ are calculated from the time series $I_{\text{center}}(t)$ and $i(t)$. The frequency labeling is in line with that of Fig. 7 and takes into account the remarks made in Sec. II A. Since $I_{\text{center}}(t)$ contains information on the self-focusing of the beam, that is, on the total phase shift Δ, the corresponding frequency is correctly labeled f_1 [e.g., Fig. 8(c)]. Furthermore, we have mentioned earlier that $i(t)$ contains only explicit information on the shape (Θ) of the polarization ellipse and its position (Φ) but *not* on the self-focusing, in distinction to the experimental $I_x(t)$ and $I_y(t)$. One recalls further that, experimentally, the use of $i(t)$, rather than $I_{x,y}(t)$, is dictated by the finiteness of δ whereas for an IPW ($\delta \to \infty$) $I_{x,y}(t)$ are the relevant quantities. Finally, since the shape of the rotating polarization

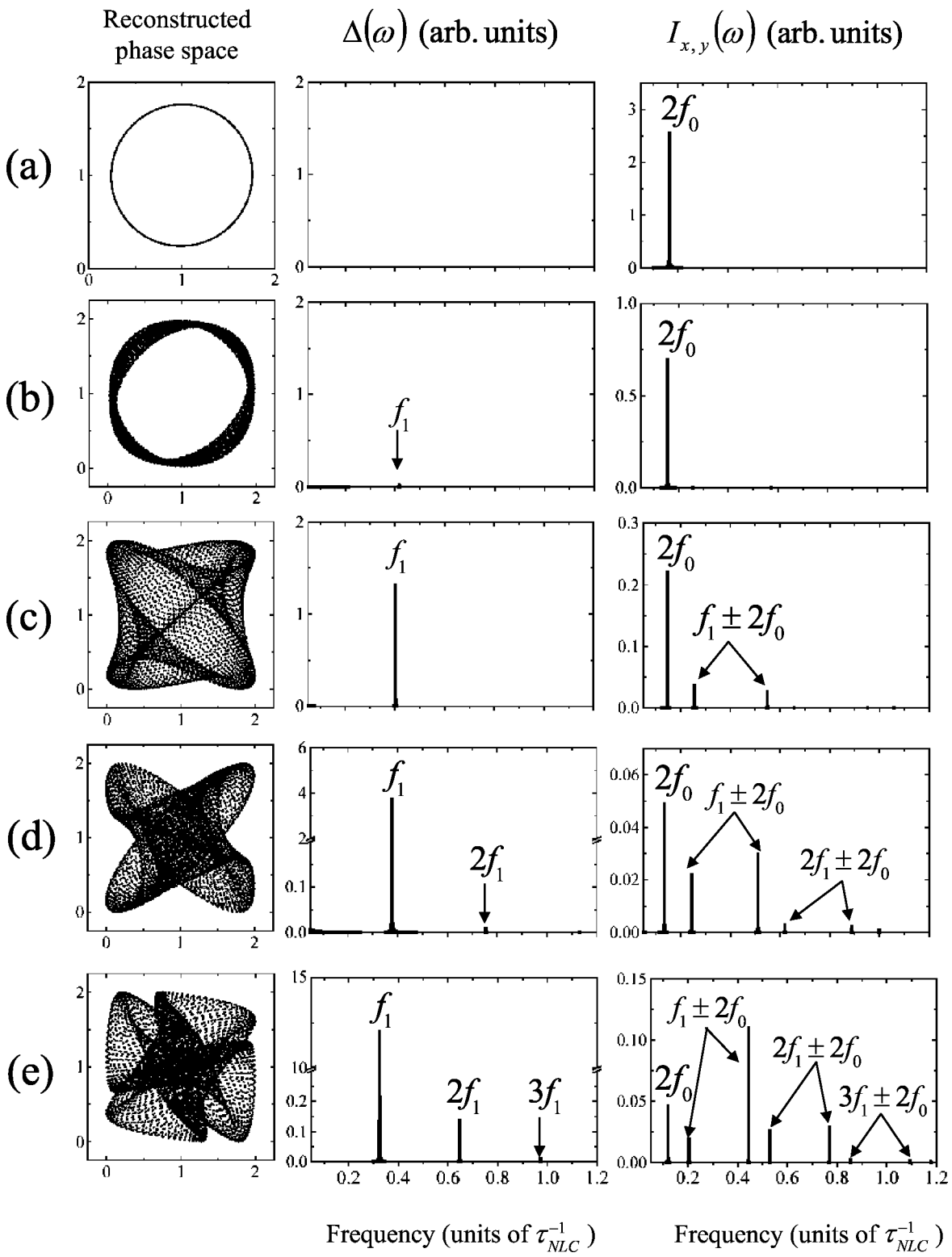

FIG. 7. Theoretical dynamical scenario in the case $L=100$ μm by retaining the first four modes of reorientation as described in Ref. [11]. From left to right: the reconstructed phase space $I_{x,y}(t+\tau)$ vs $I_{x,y}(t)$, and the Fourier power spectra of the time series $\Delta(t)$ and $I_{x,y}(t)$. The time delay is taken as $\tau=1.5\,\tau_{NLC}$. The quantity $\tau_{NLC}=\gamma L^2/K_3\pi^2$ is a characteristic reorientation time where γ is the orientational viscosity and K_3 is the Frank elastic constant associated with bend deformations. For a value of $K_3/\gamma\sim10^{-6}$ cm^2/s, typical of our sample, the numerical value of $\tau_{NLC}\sim10$ s. Frequencies are measured in units of τ_{NLC}^{-1} (~0.1 Hz). (a) $\tilde{I}=1.20$, (b) $\tilde{I}=1.45$, (c) $\tilde{I}=1.50$, (d) $\tilde{I}=1.60$, (e) $\tilde{I}=1.70$.

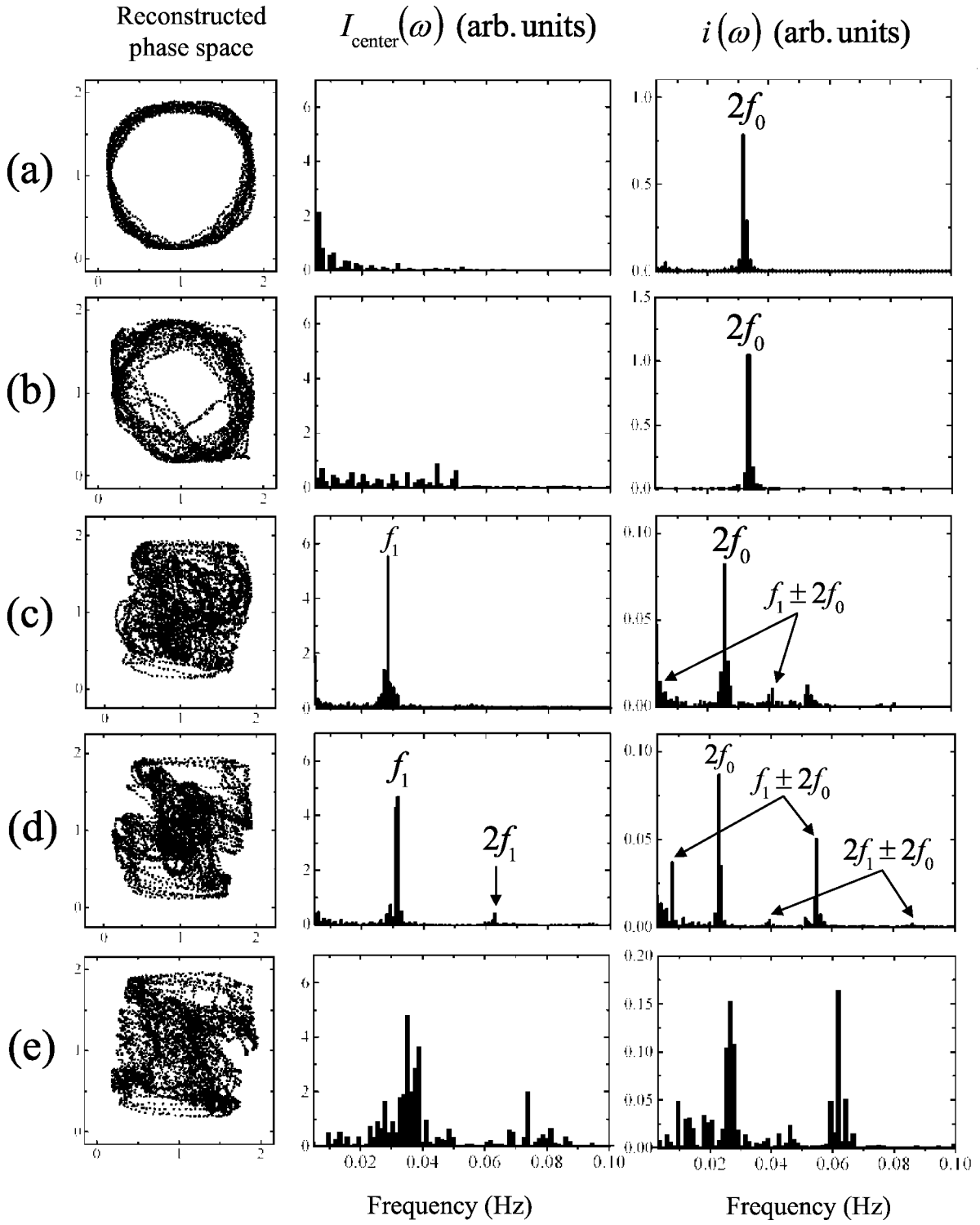

FIG. 8. Experimental dynamical scenario in the case $L=100$ μm with $\delta=0.24$. From left to right: the reconstructed phase space $i(t+\tau)$ vs $i(t)$ with $\tau=8$ s, and the Fourier power spectra of $I_{center}(t)$ and of $i(t)$. (a) $\tilde{I}=1.00$, (b) $\tilde{I}=1.10$, (c) $\tilde{I}=1.15$, (d) $\tilde{I}=1.20$, (e) $\tilde{I}=1.25$.

ellipse is almost constant in the regular precession regime the corresponding frequency of $i(\omega)$ is accordingly labeled $2f_0$ [e.g., Fig. 8(b)].

Obviously, there is a qualitative accordance between the reconstructed phase spaces in the left columns of Figs. 7 and 8. A closer look at these figures indicates similar dynamical behavior [compare Figs. 7(a)–7(d) and Figs. 8(a)–8(d)], at least for $\tilde{I}\leqslant 1.20$. For higher intensities, $\tilde{I}\geqslant 1.25$, the IPW model does not succeed to describe the experimental sequences anymore; for instance, the spectral broadening, around the discrete frequencies, shown in Fig. 8(e) is in strong contrast with the IPW situation. We have repeated this

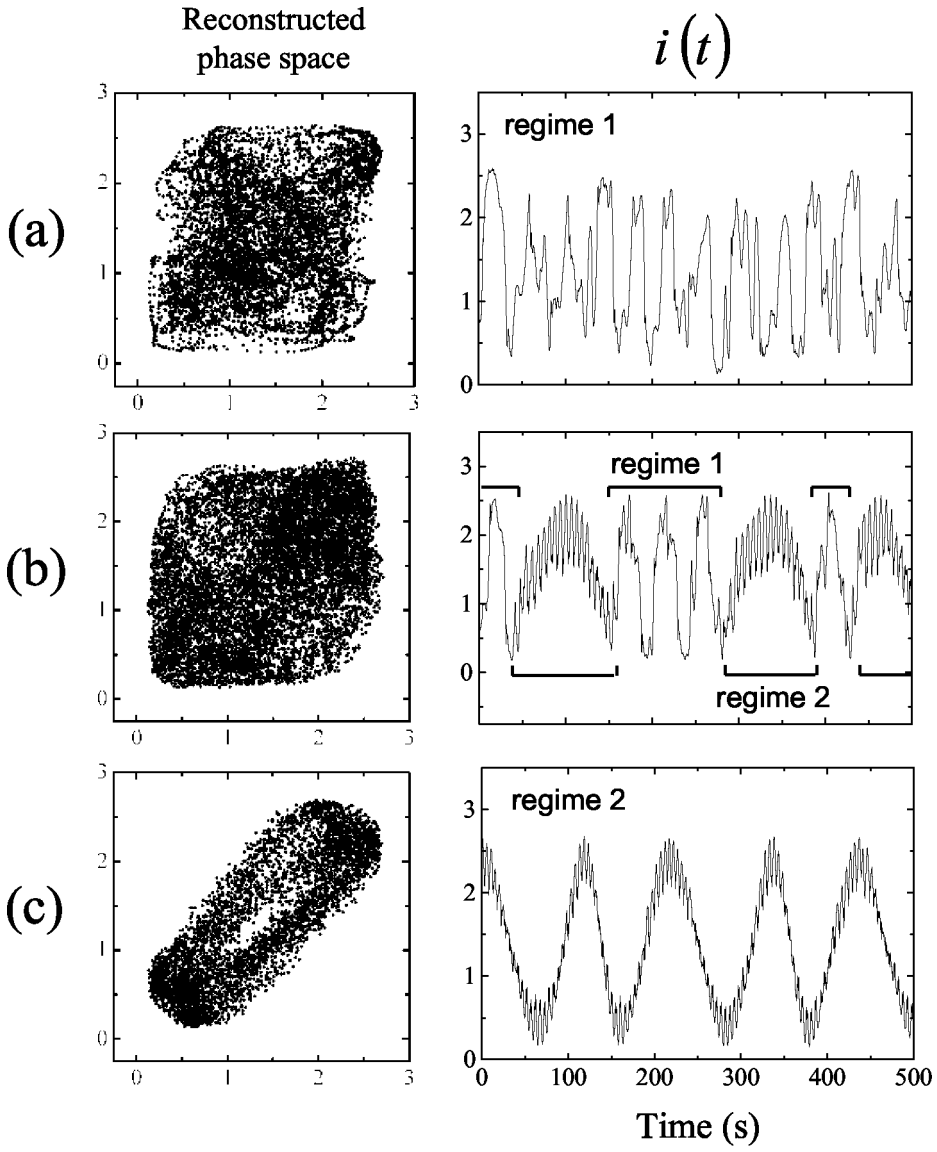

FIG. 9. Experimental reconstructed phase space $i(t+\tau)$ vs $i(t)$ for a cell thickness $L=100\,\mu$m and $\delta=0.25$, with $\tau=8$ s (left) and the corresponding time series $i(t)$ (right). (a) $\tilde{I}=1.45$, (b) $\tilde{I}=1.50$, (c) $\tilde{I}=1.55$.

experiment several times with different samples and this dynamical sequence is well reproducible. The possible chaoticity of this irregular regime is still to be determined and will be studied in future work.

2. Intermittent regime

When the intensity is increased beyond the appearance of the irregular regime [Fig. 8(e)] the system exhibits another dynamical behavior. This is illustrated in Fig. 9 where the reconstructed phase space $i(t+\tau)$ versus $i(t)$ and the time series $i(t)$ are shown for $\delta=0.25$ in the range $1.45\leqslant\tilde{I}\leqslant1.55$. At $\tilde{I}=1.45$, the irregular regime labeled ''regime 1'' in Figs. 9(a) and 9(b) is observed. At still higher intensity, this regime 1 coexists with another distinct regime labeled ''regime 2'' in Figs. 9(b) and 9(c). The system alternates between these two regimes for durations that appear almost random. At $\tilde{I}=1.55$, the system's dynamics is now definitely restricted to regime 2. This transition is associated with self-organization: it appears that the dynamics could be described with two principal frequencies (a low and a high frequency) that are clearly visible in Fig. 9(c). The high-frequency component of $i(t)$ is associated with an almost periodic large amplitude nutation with large amplitude as depicted in the signal of $I_{\text{center}}(t)$ shown in Fig. 10. We observed that these rapid pulsations correspond to cycles of expansion and contraction of several rings of self-diffraction. On the other hand, the low-frequency component corresponds to a precession regime whose frequency is several times slower than the precession rate uniform regime just above the Fréedericksz transition. This slowing down of the rotational motion is due to the fact that the effective rotational viscosity coefficient scales as $\sin^2\Theta$. Finally, in all cases, a first-order transition to a largely reoriented regime occurs when the intensity is sufficiently high as reported in previous work [8,11,29].

For beam diameter sufficiently small in comparison to the film thickness, this study points out (i) that the nutation transition is shifted to lower intensities (Fig. 6) and (ii) that new regimes of the director dynamics occur at higher intensities. The underlying physical phenomenon is, however, still

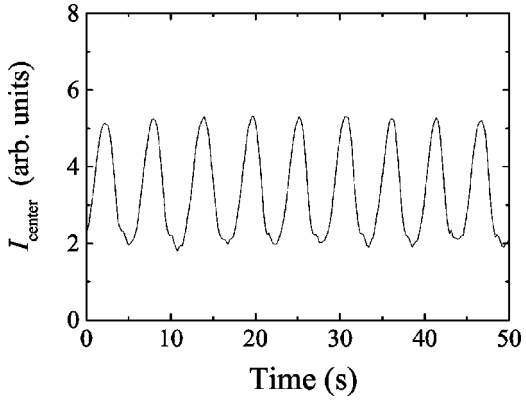

FIG. 10. Experimental time series $I_{center}(t)$ at $\tilde{I}=1.55$ for a cell thickness $L=100$ μm and $\delta=0.25$.

to be clarified and in the following section, a qualitative interpretation based on spatial walk-off between the *o* and *e* waves is proposed. Its implications from both an experimental and a theoretical point of view are also discussed.

IV. DISCUSSION

A. The role of walk-off

The physics of the problem has led us to look for an interpretation based on spatial separation of Poynting flows that occurs in optically anisotropic media and which has been found to produce instabilities in other dynamical context, e.g., laser dynamics and optical resonators (Ref. [30] and references therein). The incident flow of energy is split into an ordinary flow propagating along the *z* axis and an extraordinary one traveling at oblique incidence when the uniaxial NLC is reoriented. This situation is pictured in Fig. 11. The nonuniform walk-off $\rho(z)$ can easily be expressed as a function of the angle $\beta(z)$ between the *e*-Poynting vector and the *z* axis [Fig. 11(a)] as

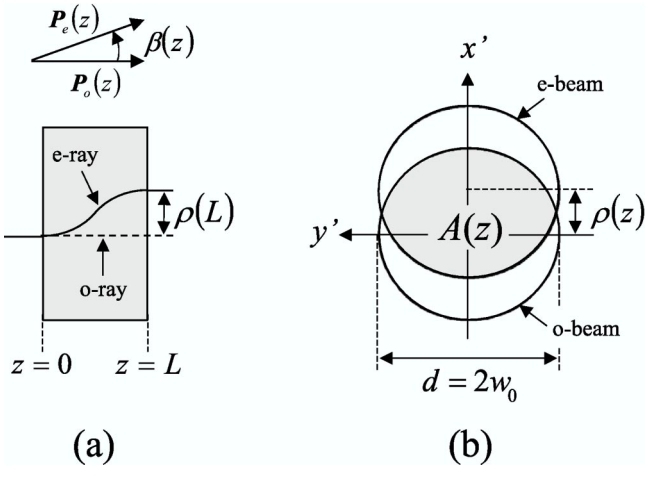

FIG. 11. (a) Representation of the Poynting flux lines (light rays in geometrical optics) for the *o* wave (dashed line) and the *e* wave (solid line) when the liquid crystal film is reoriented. $\beta(z)$ is the angle between the *o*- and *e*-Poynting vectors $\boldsymbol{P}_o(z)$ and $\boldsymbol{P}_e(z)$. The walk-off at location *z* in the film is denoted as $\rho(z)$. (b) Cross section of the *o* and *e* beams of radii w_0 at location *z* in the basis (x',y'), which is obtained from the rotation of (x,y) by an angle Φ. The shaded area $A(z)$ is the overlap area.

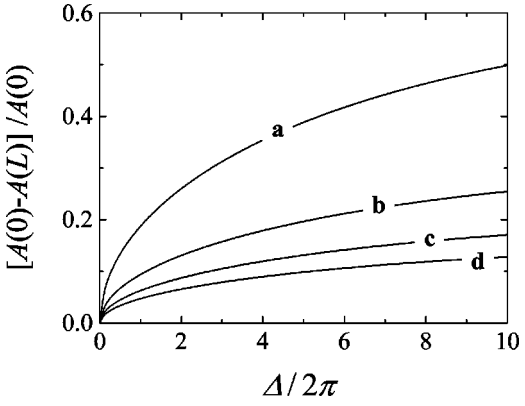

FIG. 12. Calculated relative overlap mismatch $[A(0)-A(L)]/A(0)$ vs the phase shift Δ divided by 2π for various values of δ. (a) $\delta=0.25$, (b) $\delta=0.5$, (c) $\delta=0.75$, (d) $\delta=1$. The cell thickness is $L=100$ μm.

$$\rho(z)=\int_0^z \tan[\beta(z')]dz' \tag{1}$$

and the area $A(z)$ over which the *o* and *e* beams of diameter $d=2w_0$ overlap [shaded area in Fig. 11(b)] can be written accordingly as

$$A(z)=w_0^2[\pi-2\alpha(z)-\sin 2\alpha(z)], \tag{2}$$

where

$$\alpha(z)=\arcsin\left[\frac{\rho(z)}{\delta L}\right]. \tag{3}$$

As a measure of walk-off, we choose the relative amount of mismatch of the overlap area, i.e., $[A(0)-A(L)]/A(0)$. Basically, walk-off is expected to alter significantly the director dynamics when overlap mismatch is as large as possible.

A zeroth-order approximation of the overlap mismatch can be obtained from the knowledge inferred from the IPW situation. There, the complex amplitudes of the *o* and *e* waves are written in the form $\boldsymbol{E}_o=S_o(-\sin\Phi,\cos\Phi,0)$ and $\boldsymbol{E}_e=S_e(\cos\Phi,\sin\Phi,-\tan\beta(z))$. A short calculation based on Maxwell's equation $\boldsymbol{\nabla}\cdot(\boldsymbol{\epsilon E})=0$, where the dielectric tensor at optical frequency is written as $\epsilon_{ij}=\epsilon_\perp\delta_{ij}+\epsilon_a n_i n_j$ $(\epsilon_a=\epsilon_\parallel-\epsilon_\perp)$, gives the result

$$\tan\beta(z)=\epsilon_a\sin 2\Theta/[2(\epsilon_\perp+\epsilon_a\cos^2\Theta)]. \tag{4}$$

It is seen from the preceding equations that walk-off depends not only on the geometrical ratio δ but also on the reorientation amplitude Θ. This is summarized in Fig. 12 which displays the quantity $[A(0)-A(L)]/A(0)$ versus the number of diffraction rings, $\Delta/2\pi$, for various values of δ. This figure is obtained from Eqs. (1)–(4) using the fundamental mode profile $\Theta=\Theta_0\sin(\pi z/L)$ and the relation $\Delta\simeq\tilde{L}\Theta_0^2$,

TABLE I. Experimental values of δ and the corresponding $\Delta_c/2\pi$ for different studies in various light-NLC interaction geometries. For elliptical beam shape, the notation $\delta_{\min}/\delta_{\max}$ indicates the values of δ along the minor and the major axis of the beam, respectively.

Reference	Polarization	Beam shape	Incidence angle	δ	L (μm)	$\Delta_c/2\pi$
[33]	Circular	Circular	0°	0.47	120	1.2
[10]	Circular	Circular	0°	0.75[a]	100	1.7
[12,13]	Linear (o wave)	Circular	7°	$\simeq 1$	50	2.6
[14]	Linear (o wave)	Circular	5°	0.88	50	1.9
[25–27]	Linear (o wave)	Circular	7°	0.93	75	3.3
[34]	Unpolarized	Elliptical	0°	0.6/3	50	0.82
[18]	Linear	Elliptical	0°	0.4/5.2	50	0.36
[19]	Circular	Elliptical	0°	0.32/3.2	50	0.23

[a]In Ref. [10], the beam diameter in not 60 μm but 75 μm.

which is valid in the limit $\Theta^2 \ll 1$, where the normalized length $\tilde{L}$ is defined as $\tilde{L} = L\pi\epsilon_a\epsilon_\perp^{1/2}/(2\epsilon_\parallel\lambda)$.

We believe that, even for moderate walk-off amplitude, the director dynamics could be significantly altered due to angular momentum transfer modifications arising from walk-off. Since, for a given Δ, a small δ leads to a large overlap mismatch (Fig. 12), we introduce δ_c as the typical value below which the mismatch of the overlap areas is higher than 10%, i.e., $[A(0)-A(L)]/A(0) \geqslant 0.1$. Similarly, since for a given δ, a large Δ leads to a large overlap mismatch (Fig. 12), we define Δ_c as the typical phase shift above which $[A(0)-A(L)]/A(0) \geqslant 0.1$. We can then argue that if the representation of the system in the plane (δ,Δ) lies above the line $\Delta_c(\delta)$, significant changes in the dynamics can be expected. For example, in the case of a circularly polarized excitation, it is known that $\Delta \simeq \pi$ not too far above the Fréedericksz transition, this gives $\delta_c \simeq 0.35$ for $L = 100$ μm. From a qualitative point of view, this allows us to understand the observations reported in Sec. III where $\delta \simeq 0.25$. In the light of our proposed explanation, we examine next some consequences for related studies.

B. Implications for other studies

We have summarized in Table I the values of δ used in a number of experimental studies in the field of light-induced reorientation dynamics. Following the preceding section, we report in this table the corresponding critical amount of self-focusing rings, $\Delta_c/2\pi$. On the basis of these numbers, we shall now discuss some experimental results of two interaction geometries that have received considerable attention lately and whose quantitative interpretation is still an open question.

1. Ordinary polarized excitation beam at oblique incidence

In the case of an ordinary excitation beam at oblique incidence, it has been shown theoretically that chaotic dynamics is expected and that one can even hope to observe a peculiar route to chaos through a cascade of gluing bifurcations when the intensity is used as the control parameter [15,16]. Recent experiments [14,26,25,27] seem to verify some predictions of the model, but discrepancies persist. For instance, there is clear experimental evidence for the occurrence of the first gluing bifurcation [25,27] and a signature of the second one could be found in Ref. [14], however, there is no clear sign for any further bifurcations of the cascade. Our findings with respect to the hindered cascade of harmonics [Fig. 8(e)] may provide an explanation. As seen from Table I, the corresponding experimental studies are characterized by $\Delta_c/2\pi \simeq 2-3$ although such experiments involve many rings meaning $\Delta \gg \Delta_c$. Consequently, walk-off may preclude the observation of high-order gluing bifurcation.

We suggest to perform a new set of experiments following Refs. [14,26,25,27] but with larger δ in order to get $\Delta_c > \Delta$ in the experimental range of Δ. In such a situation, one could expect to observe other steps of the cascade of gluing bifurcations towards the chaotic regime. We are, however, aware that the proximity of two successive bifurcations involves delicate experimentation since the associated intensities rapidly become smaller than the laser fluctuations.

2. Astigmatic excitation beam at normal incidence

In the case of an astigmatic excitation beam (i.e., elliptical intensity profile) at normal incidence it was shown that for large enough intensity profile ellipticity and laser power, unexpected nonlinear oscillations of the director are observed when the polarization is linear [18]. This phenomenon has been interpreted as a competition between spin and angular momentum of light deposition to the NLC film. More recently, the observation of chaotic rotation accompanied by on-off intermittency was reported in the case of a circular polarization above a certain threshold intensity [19]. One notes that this complex dynamics occurs in experimental conditions for which $\Delta_c/2\pi < 1$ (see Table I). Since the corresponding experimental reorientation satisfies $\Delta \gg 1$ [18,19], strong walk-off effects are thus expected. Our findings concerning the appearance of intriguing complex dynamics for small δ and strong laser intensity (i.e., $\Delta \gg \Delta_c$, see Sec.

III B) when the excitation beam has circular intensity profile and polarization confirms that walk-off should play a prominent role in the observations of Ref. [19].

In this view, we propose to repeat the measurements of Refs. [18,19] using the same intensity profile ellipticity but with larger beam waists. For identical reorientation amplitude this change will not modify the amount of spin and orbital momentum deposition per photon [18] while the walk-off effects will be reduced. It should then be possible to assess the contribution of the finite beam size to the observed nonlinear oscillations, chaotic rotation, and on-off intermittency.

V. CONCLUSION

We have presented the influence of the finite beam size on optically induced dynamics in nematic liquid crystals in the framework of circularly polarized light field normally incident on homeotropic sample. A new class of nonlinear dynamics driven by finite beam size has been identified. In particular, the occurrence of intermittency, self-organization, and possibly chaos has been reported. A mechanism based on walk-off between ordinary and extraordinary waves has also been proposed and its implication has been discussed in the framework of various interaction geometries.

This contribution is but a first step in understanding the influence of finite beam size effects on the molecular dynamics of nematic liquid crystals. We are planning to perform a nonlinear analysis of the experimental time series to quantitatively characterize the various regimes with respect to their dynamical properties (Lyapunov exponent, embedding analysis, noise reduction, bifurcation study, etc.). Efforts are also being made to extend the infinite plane wave modelization to include the geometrical ratio approximately in a perturbative fashion and implicitly within a full three-dimensional theory. We hope to report on these advances in the near future.

ACKNOWLEDGMENT

E.B. is grateful to K. Asatryan for his experimental support.

APPENDIX

The calculation of the optical Fréedericksz transition threshold in the field of a finite beam size has been carried out by many authors in the case of a linearly polarized excitation assuming *in-plane* reorientation profile ($\Phi=$const). For example, we mention the analytical solution proposed in Ref. [6] and the numerical solution performed in Ref. [22]. In the present case, the excitation beam is circularly polarized and it is known that the reorientation is *three dimensional* ($\Phi\neq$const) above the Fréedericksz threshold [31,32]. Nevertheless, these procedures may still apply to our case, at least for the evaluation of the threshold, since it has been demonstrated that the reorientation is quasi-in-plane in the first stage of the reorientation process when the excitation beam is circularly polarized [32]. With this in mind, we assume the same analytic dependence on δ [6] for both linearly and circularly polarized excitation as $I_F(\delta)=I_F^{\infty}(1+2\sqrt{2}/\pi\delta)^2$ where I_F^{∞} is the Fréedericksz threshold for the ideal IPW case, i.e., $\delta\rightarrow\infty$ (see dashed line in Fig. 4). On the other hand, the use of the proper numerical treatment described in Ref. [22] leads us to find the nonzero solution of the differential equation [36]

$$\frac{\partial^2 R}{\partial\tilde{r}^2}+\frac{1}{\tilde{r}}\frac{\partial R}{\partial\tilde{r}}+\beta(\tilde{r})R+\gamma(\tilde{r})R^3=0, \tag{A1}$$

where $\beta(\tilde{r})=\pi^2(\tilde{I}e^{-a\tilde{r}^2}-1)$, $\gamma(\tilde{r})=-(\pi^2/2)\tilde{I}e^{-a\tilde{r}^2}$, and $a\equiv 2/\tilde{w}_0^2$. The other dimensionless quantities are $\tilde{r}=r/L$, $\tilde{w}_0=w_0/L$, and $\tilde{I}=I_{\mathrm{tot}}/I_F^{\infty}$. Equation (A1) is associated with boundary conditions given by

$$\frac{\partial R}{\partial\tilde{r}}(0)=0,\quad R(\infty)=0, \tag{A2}$$

where $R(r)$ is the amplitude of the fundamental reorientation profile given by $\Theta(r,z)=R(r)\sin(\pi z/L)$. A careful integration of Eq. (A1) subjected to the boundary conditions given by Eq. (A2) has allowed us to extend the results of Ref. [22] to a wide range of δ values and in particular to $\delta<1$ (see solid line in Fig. 4). From Fig. 4 we see that the analytical and the numerical solutions reproduce the experimental data quite well over the interval of δ considered. The single adjustable parameter in both calculations is I_F^{∞} whose best-fit values are $I_F^{\infty}(\text{analytical})\simeq 0.60$ kW cm^{-2} and $I_F^{\infty}(\text{numerical})\simeq 0.65$ kW cm^{-2}.

[1] N.V. Tabiryan, A.V. Sukhov, and B.Y. Zel'dovich, Mol. Cryst. Liq. Cryst. **136**, 1 (1986).

[2] I.C. Khoo and S.T. Wu, *Optics and Nonlinear Optics of Liquid Crystals* (World Scientific, Singapore, 1993).

[3] E. Santamato, *Nonlinear Optical Material and Devices for Applications in Information Technology* (Kluwer Academic, Dordrecht, 1995).

[4] F. Simoni, *Nonlinear Optical Properties of Liquid Crystals and PDLC* (World Scientific, Singapore, 1997).

[5] A.S. Zolot'ko, V.F. Kitaeva, N. Kroo, N.N. Sobolev, and L. Csillag, Pis'ma Zh. Éksp. Teor. Fiz. **32**, 170 (1980) [JETP Lett. **32**, 158 (1980)].

[6] A.S. Zolot'ko, V.F. Kitaeva, V. Kuyumchyan, N. Sobolev, A. Sukhorukov, and L. Csillag, Pis'ma Zh. Éksp. Teor. Fiz. **36**, 66 (1982) [JETP Lett. **36**, 80 (1982)].

[7] B.Y. Zel'dovich and N. Tabiryan, Pis'ma Zh. Éksp. Teor. Fiz. **30**, 510 (1979) [JETP Lett. **30**, 478 (1980)].

[8] L. Marrucci, G. Abbate, S. Ferraiuolo, P. Maddalena, and E.

Santamato, Phys. Rev. A **46**, 4859 (1992).
[9] A. Vella, B. Piccirillo, and E. Santamato, Phys. Rev. E **65**, 031706 (2002).
[10] E. Brasselet, B. Doyon, T.V. Galstian, and L.J. Dubé, Phys. Lett. A **299**, 212 (2002).
[11] E. Brasselet, B. Doyon, T.V. Galstian, and L.J. Dubé, Phys. Rev. E **67**, 031706 (2003).
[12] G. Cipparrone, V. Carbone, C. Versace, C. Umeton, R. Bartolino, and F. Simoni, Phys. Rev. E **47**, 3741 (1993).
[13] N.V. Tabiryan, A.L. Tabiryan-Murazyan, V. Carbone, G. Cipparrone, C. Umeton, C. Versace, and T. Tschudi, Opt. Commun. **154**, 70 (1998).
[14] E. Santamato, P. Maddalena, L. Marrucci, and B. Piccirillo, Liq. Cryst. **25**, 357 (1998).
[15] G. Demeter and L. Kramer, Phys. Rev. Lett. **83**, 4744 (1999).
[16] G. Demeter, Phys. Rev. E **61**, 6678 (2000).
[17] G. Demeter and L. Kramer, Phys. Rev. E **64**, 020701 (2001).
[18] B. Piccirillo, C. Toscano, F. Vetrano, and E. Santamato, Phys. Rev. Lett. **86**, 2285 (2001).
[19] A. Vella, A. Setaro, B. Piccirillo, and E. Santamato, Phys. Rev. E **67**, 051704 (2003).
[20] B.Y. Zel'dovich and N. Tabiryan, Zh. Éksp. Teor. Fiz. **82**, 1126 (1982) [Sov. Phys. JETP **55**, 656 (1982)].
[21] I.C. Khoo, T.H. Liu, and R. Normandin, Mol. Cryst. Liq. Cryst. **131**, 315 (1985).
[22] I.C. Khoo, T.H. Liu, and P.Y. Yan, J. Opt. Soc. Am. B **4**, 115 (1987).
[23] V.P. Romanov and D.O. Fedorov, Opt. Spektrosk. **78**, 274 (1995) [Opt. Spectrosc. **78**, 244 (1995)].
[24] V.P. Romanov and D.O. Fedorov, Opt. Spektrosk. **79**, 313 (1995) [Opt. Spectrosc. **79**, 288 (1995)].
[25] G. Russo, V. Carbone, and G. Cipparrone, Phys. Rev. E **62**, 5036 (2000).
[26] G. Cipparrone, G. Russo, C. Versace, G. Strangi, and V. Carbone, Opt. Commun. **173**, 1 (2000).
[27] V. Carbone, G. Cipparrone, and G. Russo, Phys. Rev. E **63**, 051701 (2001).
[28] E. Santamato, B. Daino, M. Romagnoli, M. Settembre, and Y.R. Shen, Phys. Rev. Lett. **57**, 2423 (1986).
[29] E. Brasselet and T.V. Galstian, Opt. Commun. **186**, 291 (2000).
[30] M. Santagiustina, P. Colet, M. SanMiguel, and D. Walgraef, Phys. Rev. E **58**, 3843 (1998).
[31] A.S. Zolot'ko and A.P. Sukhorukov, Pis'ma Zh. Éksp. Teor. Fiz. **52**, 707 (1990) [JETP Lett. **52**, 62 (1990)].
[32] E. Brasselet and T.V. Galstian, Opt. Commun. **200**, 241 (2001).
[33] A.S. Zolot'ko, V.F. Kitaeva, N. Kroo, N.N. Sobolev, and L. Csillag, Pis'ma Zh. Éksp. Teor. Fiz. **34**, 263 (1981) [JETP Lett. **34**, 250 (1981)].
[34] L. Marrucci, F. Vetrano, and E. Santamato, Opt. Commun. **171**, 131 (1999).
[35] In Ref. [10], the beam diameter in not 60 μm but 75 μm.
[36] Reference [22] contains a number of misprints but the resulting differential equation is nevertheless correct in the case denoted by $\beta=0$.